Space-Indexed Control for Aircraft Vertical Guidance with Time Constraint

Hakim Bouadi, Felix Mora-Camino, Daniel Choukroun

Space-Indexed Control for Aircraft Vertical Guidance with Time Constraint

Hakim Bouadi[1] and Félix Mora-Camino[2]
MAIAA, Air Transport Department, ENAC, Toulouse, France, 31400

Daniel Choukroun[3]
Department of Space Engineering, Delft University of Technology, Amsterdam, Netherlands

With the growth of civil aviation traffic capacity, safety and environmental considerations urge today for the development of guidance systems with improved accuracy for spatial and temporal trajectory tracking. This should induce increased practical capacity by allowing timely operations at minimum separation standards while at take-off and landing, trajectory dispersion should be reduced, resulting in better controlled noise impacts on airport surrounding communities. Current civil aviation guidance systems operate with real time corrective actions to maintain the aircraft trajectory as close as possible to a space-indexed planned trajectory while the flight management system copes indirectly with overfly time constraints. In this paper, we consider the design of new longitudinal guidance laws so that accurate vertical tracking is achieved while overfly time constraints are satisfied. Here, distance to land is adopted as the independent variable for the aircraft flight dynamics since it is today available on board aircraft with acceptable accuracy. A representation of aircraft longitudinal guidance dynamics is developed according to this spatial variable and a space-indexed nonlinear inverse control law is established to make the aircraft follow accurately a vertical profile and a desired airspeed. The desired airspeed is defined by an outer space-indexed control loop to make the aircraft overfly different waypoints according to a

---

[1] PhD, Air Transport Department, 07, Avenue Edouard Belin, Toulouse, 31400/hakimbouadi@yahoo.fr.
[2] Professor, Air Transport Department, Head of Automation Research Group, 07, Avenue Edouard Belin, Toulouse, 31400/Felix.Mora@enac.fr, moracamino@hotmail.fr.
[3] Associate Professor, Department of Space Engineering, Delft University of Technology, Kluyverweg 1, 2629 HS Delft, The Netherlands, D.Choukroun@tudelft.nl.

planned time-table. Numerical simulation experiments with different wind conditions for a transportation aircraft performing a descent approach for landing under this new guidance law are described. The resulting guidance performances are compared with those obtained from a classical time-based guidance control law.

Nomenclature

x = longitudinal displacement, m

z = altitude, m

V_a = airspeed, m/s

V_G = ground speed, m/s

γ_a = flight path angle w.r.t airspeed, rad

θ = pitch angle, rad

α = angle of attack, rad

L = lift force, N

D = drag force, N

T = thrust force, N

C_L = lift force coefficient

C_D = drag force coefficient

m = mass, Kg

q = pitch rate, rad/s

M = pitch moment, N.m

C_m = pitch moment coefficient

I_y = pitch inertia moment, Kg.m^2

ρ = air density, Kg/m^3

S = wing surface area, m^2

g = gravity acceleration, m/s^2

τ = engine time constant , s

δ_{th} = throttle setting , rad

δ_e = elevator deflection , rad

w_x = longitudinal wind component , m/s

w_z = vertical wind component , m/s

I. Introduction

World air transportation traffic has known a sustained increase over the last decades leading to airspace near saturation in large areas of developed and emerging countries. For example, today up to 27,000 flights cross European airspace every day while the number of passengers is expected to double by 2020. Then safety and environmental considerations urge today for the development of new guidance systems providing improved accuracy for spatial and temporal trajectory tracking.

In the near future air traffic management environment defined by SESAR (Single European Sky ATM Research) and NextGen (Next Generation Air Transportation System) projects, aircraft will progress in four dimensions, sharing accurate airborne predictions with the ground systems, and being able to meet time constraints at specific waypoints with high precision when the traffic density requires it [1, 2]. Then better separation and sequencing of traffic flows will be possible while green climb/descent trajectories will be eased in terminal areas.

Current civil aviation guidance systems generate real time control actions to maintain the aircraft trajectory as close as possible to a planned trajectory provided by the Flight Management System or to comply with ATC tactical demands based either on spatial or temporal considerations [3, 4]. While wind remains one of the main causes of guidance errors [5–7], these new requirements for improved ATC are attended with relative efficiency by current airborne guidance systems. These guidance errors are detected by navigation systems whose accuracy has known large improvements in the last decade with the hybridization of inertial units with Global Positioning System information. Nevertheless, until today vertical guidance needs improved performances [8, 9] and corresponding errors especially during manoeuvre [10] may remain large considering the time-based control laws which are applied by flight guidance systems [11].

In this paper, we propose a new approach to design vertical guidance control laws so that accurate vertical tracking and overfly time are insured. Instead of using time as the independent variable to represent the guidance dynamics of the aircraft, we adopt distance to land, which can be considered today to be available online with acceptable accuracy and availability. A different representation of aircraft vertical guidance dynamics is developed according to this spatial variable where the overfly time becomes a controlled variable. Then a nonlinear inverse control law based-on

this new proposed spatial representation of guidance dynamics is established to make the aircraft follow accurately a vertical profile and a desired airspeed [12–14]. This leads to regulate on a space-indexed basis the desired airspeed to meet constraints related to the stall speed and the maximum operating speed while making the aircraft to overfly different waypoints according to a planned time-table.

Simulation experiments with different wind conditions are realized for a transportation aircraft performing a direct descent approach for landing under this new guidance law. The resulting guidance performances are compared with those obtained from an equivalent time-based guidance control law.

II. Aircraft Longitudinal Flight Dynamics

The motion of an approach/descent transportation aircraft along a landing trajectory is referenced with respect to a Runway Reference Frame (RRF) where its origin is located at the runway entrance as shown in Fig. 1.

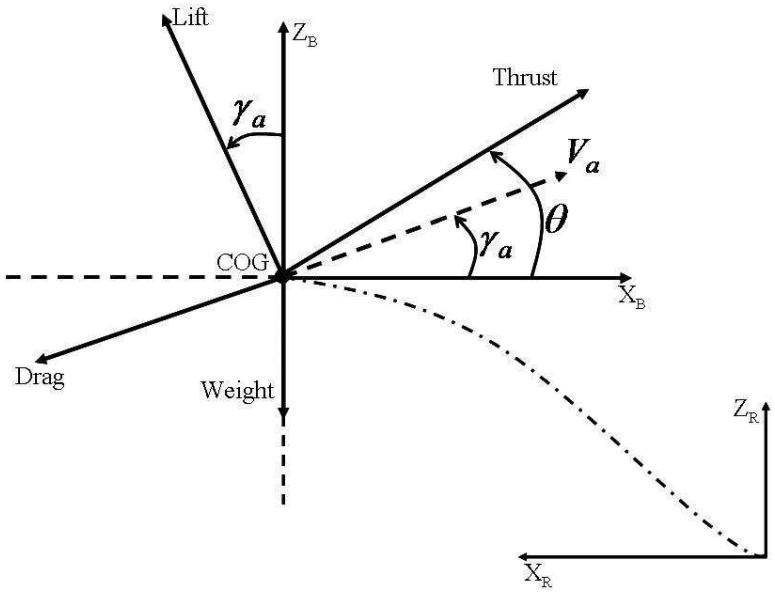

Fig. 1 Aircraft attitude and acting forces.

A. Classical Longitudinal Flight Dynamics

The vertical plane components of the inertial speed are such as:

$$\dot{x} = -V_a \cos\gamma_a + w_x \tag{1a}$$

$$\dot{z} = V_a \sin\gamma_a + w_z \tag{1b}$$

where x and z are the vertical plane coordinates of the aircraft centre of gravity in the RRF, V_a is the airspeed modulus, γ_a is the flight path angle, w_x and w_z are the wind components in the RRF.

The airspeed and the flight path angle are given by:

$$V_a = \sqrt{(\dot{x} - w_x)^2 + (\dot{z} - w_z)^2} \tag{2a}$$

$$\gamma_a = -\arctan\left(\frac{\dot{z} - w_z}{\dot{x} - w_x}\right) \tag{2b}$$

Adopting classical assumptions such as the RRF being an inertial frame, local flatness of the Earth, constant aircraft mass, the translational acceleration equations can be written as:

$$m\ddot{x} = -T\cos\theta + D(z, V_a, \alpha)\cos\gamma_a + L(z, V_a, \alpha)\sin\gamma_a \tag{3a}$$

$$m\ddot{z} = T\sin\theta - D(z, V_a, \alpha)\sin\gamma_a - mg + L(z, V_a, \alpha)\cos\gamma_a \tag{3b}$$

with T, D and L are respectively the thrust, drag and lift forces, α denotes the angle of attack:

$$\alpha = \theta - \gamma_a \tag{4}$$

The lift and drag forces are given by:

$$L = \frac{1}{2}\rho(z)V_a^2 S C_L \qquad \text{with} \qquad C_L = C_{L_0} + C_{L_\alpha}\alpha \tag{5a}$$

$$D = \frac{1}{2}\rho(z)V_a^2 S C_D \qquad \text{with} \qquad C_D = C_0 + C_1\alpha + C_2\alpha^2 \tag{5b}$$

where $\rho(z)$, S, C_L and C_D represent the air density with respect to the altitude, the wing surface area, the lift and drag coefficients, respectively. C_{L_0}, C_{L_α}, C_0, C_1 and C_2 are aerodynamic coefficients. Assuming first order dynamics with time constant τ for the thrust delivered by the engines, we get:

$$\dot{T} = \frac{1}{\tau}(\delta_{th} - T) \tag{6}$$

Under the above assumptions, the pitch rate dynamics is described by the following state equations:

$$\dot{\theta} = q \qquad \text{with} \qquad \dot{q} = \frac{M}{I_y} \tag{7}$$

where M, I_y denote respectively the pitch moment and inertia moment according to the aircraft lateral axis where M is given by:

$$M = \frac{1}{2}\rho(z)V_a^2 S\overline{c}C_m \qquad \text{with} \qquad C_m = C_{m_0} + C_{m_\alpha}\alpha + C_{m_q}\frac{q\overline{c}}{2V_a} + C_{m_{\delta_e}}\delta_e \tag{8}$$

where C_{m_0}, C_{m_α}, C_{m_q} and $C_{m_{\delta_e}}$ are non-dimensional stability derivatives. From Eq. (3a) and Eq. (3b), state equations of airspeed and flight path angle with respect to airspeed can be rewritten such as:

$$\dot{V}_a = \frac{1}{m}\Big[T\cos\alpha - D(z, V_a, \alpha) - mg\sin\gamma_a + m\Big(\dot{w}_x\cos\gamma_a - \dot{w}_z\sin\gamma_a\Big)\Big] \tag{9a}$$

$$\dot{\gamma}_a = \frac{1}{mV_a}\Big[T\sin\alpha + L(z, V_a, \alpha) - mg\cos\gamma_a - m\Big(\dot{w}_x\sin\gamma_a + \dot{w}_z\cos\gamma_a\Big)\Big] \tag{9b}$$

The time-indexed longitudinal flight dynamics are given by Eq. (1a), Eq. (1b), Eq. (6), Eq. (7), Eq. (9a) and Eq. (9b). The independent control inputs to the above flight dynamics are chosen here to be the pitch rate q and the throttle setting δ_{th} while w_x and w_z are perturbation inputs.

B. Space-Indexed Longitudinal Flight Dynamics

Considering that during an approach/descent manoeuver without holdings the distance-to-land time function $x(t)$ is invertible, it is possible to express during these manoeuvers all the flight variables with respect to x and its derivatives instead of time t. It is possible to write for any variable $(*)$:

$$\frac{d*}{dx} = \frac{d*}{dt}.\frac{dt}{dx} = \frac{1}{V_G}.\frac{d*}{dt} \tag{10}$$

where the ground speed at position x and time t is given by:

$$V_G = \frac{dx}{dt} = -V_a\cos\gamma_a + w_x \tag{11}$$

The first, second and third time-derivative of variable (x) are written $(\dot{x},\ \ddot{x},\ \dddot{x})$, respectively. Whereas, the k^{th} derivative of variable $(*)$ with respect to x is written $(*^{[k]})$ and Eq. (1a), Eq.

(1b), Eq. (6), Eq. (7), Eq. (9a) and Eq. (9b) are rewritten as:

$$z^{[1]} = \frac{dz}{dx} = \frac{dz}{dt}.\frac{dt}{dx} = \frac{V_a \sin\gamma_a + w_z}{V_G} \tag{12a}$$

$$\theta^{[1]} = \frac{q}{V_G} \tag{12b}$$

$$q^{[1]} = \frac{M}{I_y V_G} \tag{12c}$$

$$T^{[1]} = \frac{\delta_{th} - T}{\tau V_G} \tag{12d}$$

$$V_a^{[1]} = \frac{1}{mV_G}\left[T\cos\alpha - D(z, V_a, \alpha) - mg\sin\gamma_a + m\left(\dot{w}_x \cos\gamma_a - \dot{w}_z \sin\gamma_a\right)\right] \tag{12e}$$

$$\gamma_a^{[1]} = \frac{1}{mV_a V_G}\left[T\sin\alpha + L(z, V_a, \alpha) - mg\cos\gamma_a - m\left(\dot{w}_x \sin\gamma_a + \dot{w}_z \cos\gamma_a\right)\right] \tag{12f}$$

with the additioanl equation:

$$t^{[1]} = \frac{1}{V_G} \tag{13}$$

III. Vertical Trajectory Tracking Control Objectives

Two main guidance objectives have been considered in this study:

1. To follow accurately a space-referenced vertical profile $z_d(x)$ which possibly has been generated by the flight management system, in accordance with economic and environmental objectives and constraints,

2. To respect a desired time table $t_d(x)$ for the progress of the aircraft towards the runway or any other reference point.

The desired time table as well as the desired vertical profile should be generated for the whole flight by the flight management system in charge of finding a trajectory meeting satisfactorily economic objectives (expressed in general in terms of fuel consumption and flight time) and air traffic management constraints while flight domain (height and speed limits) constraints must be satisfied.

Trying to meet directly the second objective in presence of wind can lead to hazardous situations with respect to airspeed limits. So this second objective is taken into account through the on-line definition of a desired airspeed to be followed by the aircraft. In this study, it is supposed that accurate online estimates of wind parameters are available [5].

From the desired time table $t_d(x)$, we get a desired ground speed $V_{G_d}(x)$:

$$V_{G_d}(x) = 1/\frac{dt_d}{dx}(x) \tag{14}$$

then, taking into account an estimate of the longitudinal component of wind speed, a space-referenced desired airspeed $V_{a_d}(x)$ can be defined with the consideration of lower and upper limits for the airspeed:

- For lower speeds, the stall speed V_S plus a margin ΔV_{min} must be introduced:

$$V_{a_d}(x) = max\Big\{V_S(z_d(x)) + \Delta V_{min}, V_{G_d}(x) - \hat{w}_x(x)\Big\} \tag{15}$$

  where $\hat{w}_x$ is the estimate of the horizontal wind speed.

- For higher speeds, the maximum operating speed V_{MO} must be introduced:

$$V_{a_d}(x) = min\Big\{V_{MO}(z_d(x)), V_{G_d}(x) - \hat{w}_x(x)\Big\} \tag{16}$$

- In all other cases:

$$V_{a_d}(x) = V_{G_d}(x) - \hat{w}_x(x) \tag{17}$$

Then considering that q and δ_{th} are the control inputs while z and V_a are the controlled outputs, we can derive Eq. (12a) and Eq. (12e) with respect to space until we get:

$$V_a^{[2]} = \frac{1}{V_G^2}\Big[A_V(z,\alpha,V_a,T,W) + B_{V_q}(z,\alpha,V_a,T,W)q + B_{V_T}(z,\alpha,V_a,T,W)\delta_{th}\Big] \tag{18a}$$

$$z^{[3]} = \frac{1}{V_G^2}\Big[A_z(z,\alpha,V_a,T,W) + B_{z_q}(z,\alpha,V_a,T,W)q + B_{z_T}(z,\alpha,V_a,T,W)\delta_{th}\Big] \tag{18b}$$

where W represents the parameters w_x, w_z, $\dot{w}_x$, $\dot{w}_z$ and $\ddot{w}_x$, $\ddot{w}_z$ which can be expressed successively. The exact expressions of components A_V, B_{V_q}, B_{V_T} and A_z, B_{z_q}, B_{z_T} in Eq. (18a) and Eq. (18b) are shown in Appendix. 1.

Since the B_i terms are in general different from zero, the relative degrees [13] of the output variables V_a and z are equal respectively to 1 and 2. According to these values, there are no internal dynamics to worry about in the present case since stabilizing the output variables along a smooth trajectory will imply the stabilization of all other state variables.

IV. Space-Indexed Against Time-Indexed Reference Trajectories

In the literature, countless control techniques have been designed for aircraft trajectory tracking using time as the independent variable [15] while quite nothing has been published until recently with space as the independent variable [13, 14]. However, many ATC solicitations to aircraft guidance can be considered to introduce space based constraints (time separation at a given waypoint, continuous descent approaches, time metered approaches for optimal use of runways, etc). The use of classical time-indexed guidance systems in these situations appears to contribute to the Flight Technical Error (FTE) of the guidance system. Then, to display the interest for this new approach, in this section it is shown how for general aircraft operations linear decoupled space and time-indexed guidance dynamics are not always equivalent.

Considering the relative degrees of and, nonlinear inverse control techniques [13, 14] can be used to make these guidance variables satisfy decoupled linear spatial dynamics such as:

$$\sum_{k=0}^{2} a_k^V \left(V_a - V_{a_d} \right)^{[k]} = 0 \tag{19a}$$

$$\sum_{k=0}^{3} a_k^z \left(z - z_d \right)^{[k]} = 0 \tag{19b}$$

where the corresponding characteristic polynomials $\sum_{k=0}^{2} a_k^V s^k$ and $\sum_{k=0}^{3} a_k^z s^k$ are chosen to be asymptotically stable with adequate transients and response times.

According to derivation rules for composed functions, we get:

$$\xi_z^{[1]} = \frac{\dot{\xi}_z}{V_G} \tag{20a}$$

$$\xi_z^{[2]} = \frac{1}{V_G^2} \left(\ddot{\xi}_z - \frac{\dot{\xi}_z \dot{V}_G}{V_G} \right) \tag{20b}$$

$$\xi_z^{[3]} = \frac{1}{V_G^3} \left[\dddot{\xi}_z - 3\ddot{\xi}_z \frac{\dot{V}_G}{V_G} + \dot{\xi}_z \left(3\frac{\dot{V}_G^2}{V_G^2} - \frac{\ddot{V}_G}{V_G} \right) \right] \tag{20c}$$

and

$$\xi_{V_a}^{[1]} = \frac{\dot{\xi}_{V_a}}{V_G} \tag{21a}$$

$$\xi_{V_a}^{[2]} = \frac{1}{V_G^2} \left(\ddot{\xi}_{V_a} - \frac{\dot{\xi}_{V_a} \dot{V}_G}{V_G} \right) \tag{21b}$$

with $\xi_z(x)$ and $\xi_{V_a}(x)$ being the tracking errors related to the desired altitude $z_d(x)$ and to the

desired airspeed profile $V_{a_d}(x)$, respectively:

$$\xi_z(x) = z(x) - z_d(x) \tag{22a}$$

$$\xi_{V_a}(x) = V_a(x) - V_{a_d}(x) \tag{22b}$$

Then Eq. (19a) and Eq. (19b) can be rewritten as follows:

$$\xi_{V_a}^{[2]}(x) + k_{1v}\xi_{V_a}^{[1]}(x) + k_{2v}\xi_{V_a}(x) = 0 \tag{23a}$$

$$\xi_z^{[3]}(x) + k_{1z}\xi_z^{[2]}(x) + k_{2z}\xi_z^{[1]}(x) + k_{3z}\xi_z(x) = 0 \tag{23b}$$

where $k_{1v}, k_{2v}, k_{1z}, k_{2z}$ and k_{3z} are real parameters such as the roots of $s^2 + k_{1v}s + k_{2v}$ and $s^3 + k_{1z}s^2 + k_{2z}s + k_{3z}$ produce adequate tracking error dynamics (convergence without oscillation in accordance with a given space segment) with s denoting Laplace variable.

It appears that when replacing in Eq. (23a) and Eq. (23b) the space derivatives of the outputs by the expressions given by Eq. (20a) to Eq. (21b), we get nonlinear coupled time dynamics for the altitude and the airspeed errors. Only in the case of a constant ground speed where the space and temporal derivatives are related by:

$$\xi_z^{[k]} = \frac{\xi_z^{(k)}}{V_G^k} \tag{24a}$$

$$\xi_{V_a}^{[k]} = \frac{\xi_{V_a}^{(k)}}{V_G^k} \tag{24b}$$

we get equivalent linear decoupled time dynamics given by:

$$\dddot{\xi}_z + k_{1z}V_G\ddot{\xi}_z + k_{2z}V_G^2\dot{\xi}_z + k_{3z}V_G^3\xi_z = 0 \tag{25a}$$

$$\ddot{\xi}_{V_a} + k_{1v}V_G\dot{\xi}_{V_a} + k_{2v}V_G^2\xi_{V_a} = 0 \tag{25b}$$

This case corresponds to a no wind situation where the airspeed of the aircraft is maintained constant.

In the case where $\dot{V}_G$ remains constant (i.e. $V_G(t) = V_G(t_0) + \dot{V}_G.(t - t_0)$) over a time (space) span starting at t_0, Eq. (25a) and Eq. (25b) become:

$$\dddot{\xi}_z + \left(k_{1z}V_G - 3\frac{\dot{V}_G}{V_G}\right)\ddot{\xi}_z + \left(k_{2z}V_G^2 - k_{1z}\dot{V}_G + 3\frac{\dot{V}_G^2}{V_G^2}\right)\dot{\xi}_z + k_{3z}V_G^3\xi_z = 0 \tag{26a}$$

$$\ddot{\xi}_{V_a} + \left(k_{1v}V_G - \frac{\dot{V}_G}{V_G}\right)\dot{\xi}_{V_a} + k_{2v}V_G^2\xi_{V_a} = 0 \tag{26b}$$

then the above decoupled dynamics have time variant parameters and the predictivity (time of response) of these dynamics is lost. It can be however shown that if $\dot{V}_G$ is very small with respect to V_G, these dynamics remain stable.

Then the adoption of time based reference trajectories are of interest when guidance requirements can be better expressed with respect to space (especially when time constraints at specific waypoints are considered). Then it appears that adopting in this case a space based trajectory tracking technique should avoid this source of error.

V. Space-Indexed Nonlinear Dynamic Inversion Control Laws

In this section the space-indexed nonlinear dynamic inversion control technique introduced in [12–14] to perform aircraft trajectory tracking is displayed. The desired vertical profile $z_d(x)$ is supposed to be a smooth function of x (in the considered application x is the distance to touchdown) while considering expressions of airspeed constraints in Eq. (15), Eq. (16) and Eq. (17), V_{a_d} is supposed to be a piecewise smooth function of x.

Since in general flight conditions the control matrix given by:

$$\Gamma = \begin{pmatrix} B_{z_q} & B_{z_T} \\ B_{V_q} & B_{V_T} \end{pmatrix} \tag{27}$$

is invertible [13, 14], it is possible to perform the dynamic inversion to get effective trajectory tracking control laws [10, 11]. So we get:

$$\begin{pmatrix} q_d(x) \\ \delta_{th}(x) \end{pmatrix} = \Gamma^{-1} \begin{pmatrix} V_G^2 D_z(x) - A_z \\ V_G^2 D_{V_a}(x) - A_V \end{pmatrix} \tag{28}$$

with:

$$D_z(x) = z_d^{[3]}(x) + k_{1z}\xi_z^{[2]}(x) + k_{2z}\xi_z^{[1]}(x) + k_{3z}\xi_z(x) \tag{29a}$$

$$D_{V_a}(x) = V_{a_d}^{[2]}(x) + k_{1v}\xi_{V_a}^{[1]}(x) + k_{2v}\xi_{V_a}(x) \tag{29b}$$

Observe here that while the successive spatial derivatives of desired outputs $z_d(x)$ and $V_{a_d}(x)$ can be directly computed, the successive spatial derivatives of actual outputs $z(x)$ and $V_a(x)$ in Eq. (29a) and Eq. (29b) can be computed from Eq. (12a) to Eq. (12f) where the wind parameters

must be replaced by their estimates. This yields, the control scheme displayed in Fig. 2 where the autopilot operates in the temporal frame to control aircraft attitude while the auto-guidance operates in the space frame.

In order to make the aircraft overfly different waypoints according to a planned time-table $t_d(x)$, a simple outer-loop PID controller is introduced. Desired airspeed is computed and regulated to meet constraints related basically to the desired ground speed $V_{G_d}(x)$, the minimum allowable speed and the maximum operating speed. Desired ground speed is defined based on the reference time-table $t_d(x)$ according to Eq. (14). Then the PID speed versus space controller is expressed as:

$$u_t(x) = K_p e_t(x) + K_d \frac{de_t}{dx}(x) + K_i \int_{x-\Delta x}^{x} e_t(\Theta) d\Theta \tag{30}$$

where Δx is small space interval and:

$$e_t(x) = t(x) - t_d(x) \tag{31}$$

and

$$V_{a_d}^C(x) = V_{a_d}(x) + u_t(x) \tag{32}$$

The corrected desired airspeed $V_{a_d}^C$ must also satisfy the airspeed constraints defined in Eq. (15), Eq. (16) and Eq. (17).

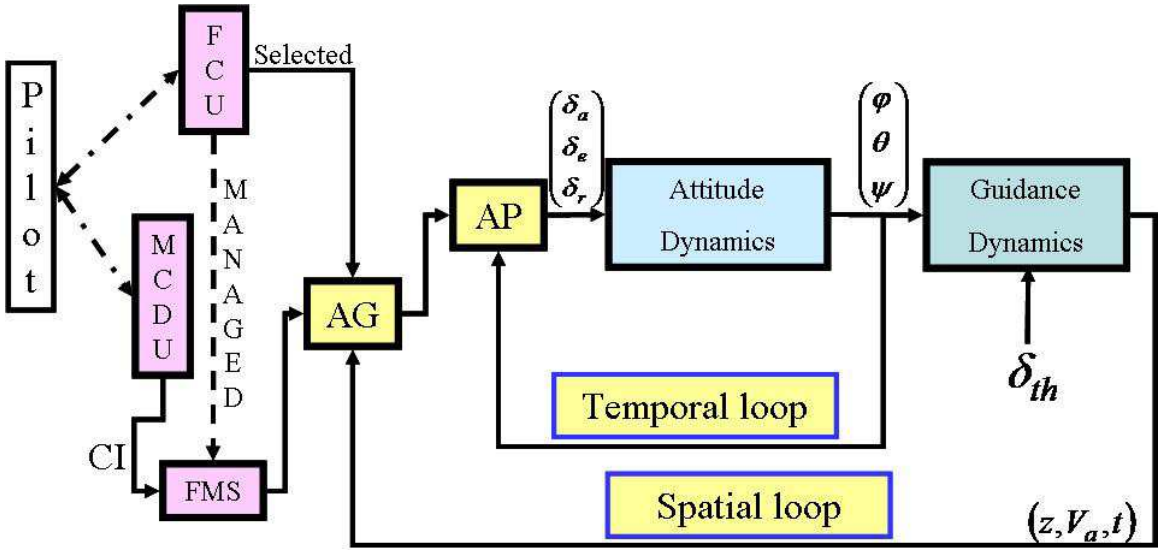

Fig. 2 Proposed flight control structure

VI. Simulation Study of Longitudinal Guidance

One of the objectives to be met when applying a space-indexed NDI control to the longitudinal guidance dynamics of an aircraft is to make the vertical tracking error follows dynamics as defined by Eq. (23a) and Eq. (23b) (convergence without oscillation over a given space segment). This objective traduced in the time frame leads to the tracking error dynamics of Eq. (25a) and Eq. (25b) which are adopted here to apply the time-indexed NDI control and then perform a fair comparison.

The proposed guidance approach is illustrated using the Research Civil Aircraft Model (RCAM) which has the characteristics of a wide body transportation aircraft [15] with a maximum allowable landing mass of about 125 tons with a nominal landing speed of 68m/s. There, the control signals are submitted to rate limits and saturations as follows:

$$-25\frac{\pi}{180}rad \leqslant \delta_e \leqslant 10\frac{\pi}{180}rad \tag{33a}$$

$$-15\frac{\pi}{180}rad/s \leqslant \dot{\delta}_e \leqslant 15\frac{\pi}{180}rad/s \tag{33b}$$

$$0.5\frac{\pi}{180}rad \leqslant \delta_{th} \leqslant 10\frac{\pi}{180}rad \tag{33c}$$

$$-1.6\frac{\pi}{180}rad/s \leqslant \dot{\delta}_{th} \leqslant 1.6\frac{\pi}{180}rad/s \tag{33d}$$

while the minimum allowable speed is $1.23 \times V_{stall}$ with $V_{stall} = 51.8$m/s and the angle of attack is limited to the interval $[-11.5°, 18°]$ where $\alpha_{stall} = 18°$.

A. Simulation Results in No Wind Condition

Here the performances obtained for vertical guidance from the space-indexed NDI and those obtained from the time-indexed NDI are compared in no wind situation.

Figure. 3(a) and Fig. 3(b) display respectively altitude tracking performances resulting from time-indexed NDI and space-indexed NDI guidance schemes. While Fig. 4(a) and Fig. 4(b) provide closer views of altitude and tracking performance during initial transients, it appears clearly that in both cases the spatial-indexed NDI trajectory tracking technique provides better results: the spatial span for convergence towards the desired trajectories is shortened by about 2000m while convergence is performed with reduced oscillations. Figures. 5(a) and 5(b) display respectively airspeed tracking performances by space-indexed NDI and time-indexed NDI guidance schemes when the aircraft is

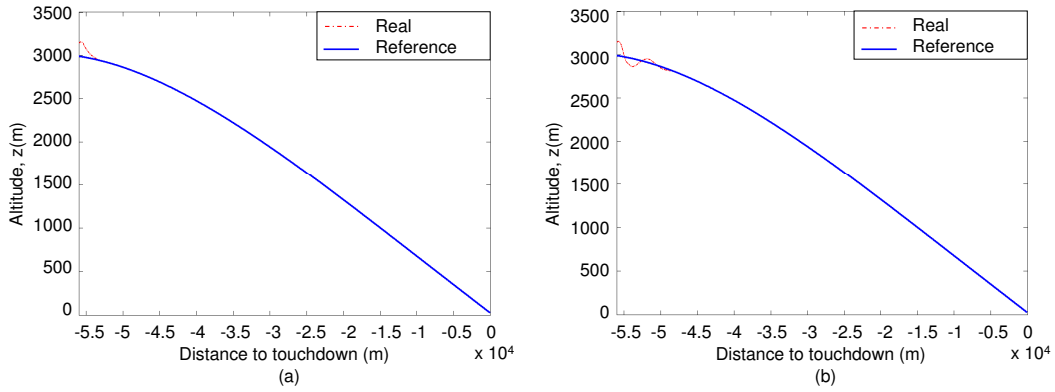

(a) Space-indexed NDI (b) Time-indexed NDI

Fig. 3 Altitude trajectory tracking performance by space-indexed (a) and time-indexed (b) NDI in no wind condition.

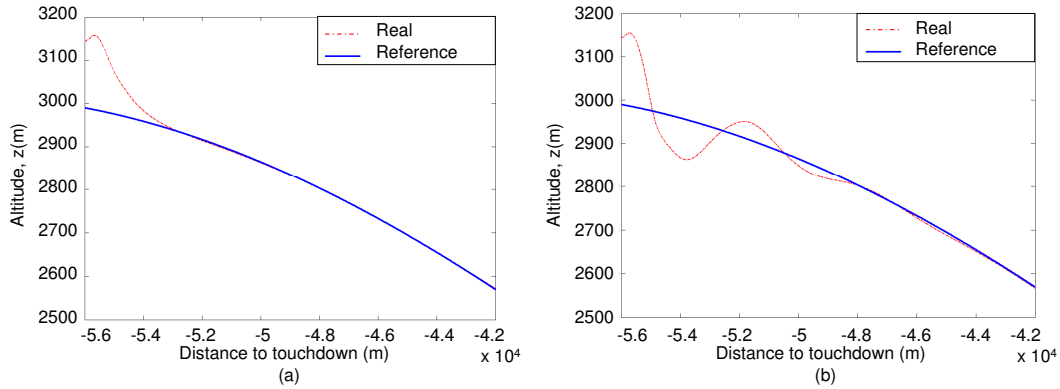

(a) Space-indexed NDI (b) Time-indexed NDI

Fig. 4 Initial altitude tracking by space-indexed (a) and time-indexed (b) NDI in no wind condition.

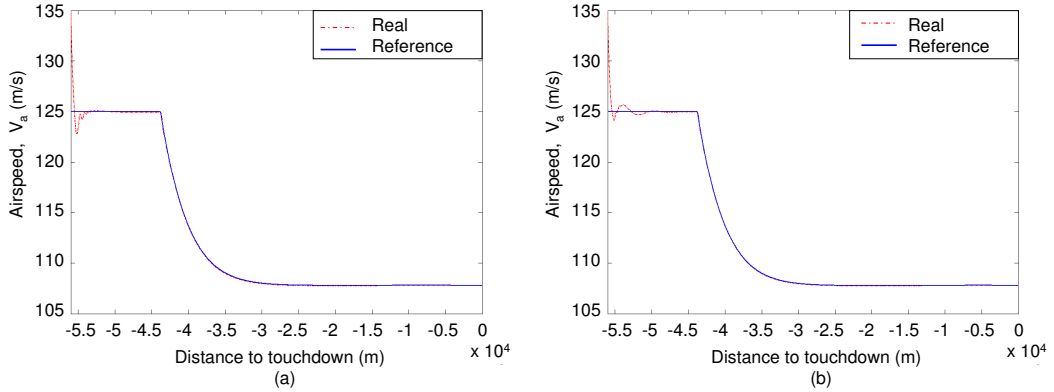

(a) Space-indexed NDI (b) Time-indexed NDI

Fig. 5 Airspeed profile tracking performance by space-indexed (a) and time-indexed (b) NDI in no wind condition.

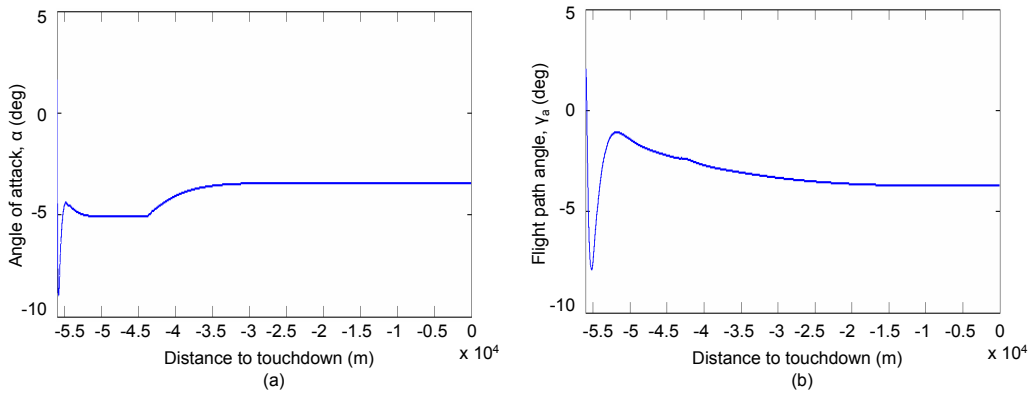

(a) Space-indexed NDI

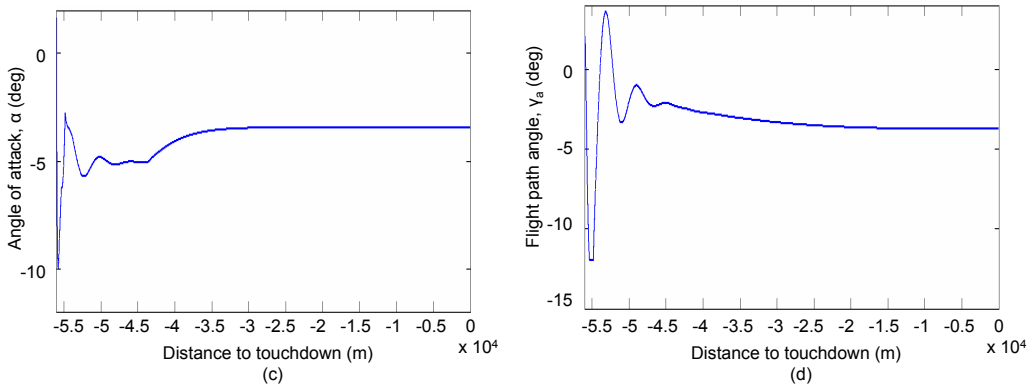

(b) Time-indexed NDI

Fig. 6 Angle of attack and flight path angle evolution by space-indexed (a) and time-indexed (b) NDI in no wind condition.

initially late according to the planned time table. It appears clearly that the aircraft increases its airspeed to the maximum operating speed during 12000m until it catches up its delay.

Since except at initial transients the performances look similar, Fig. 6(a), Fig. 6(b), Fig.7(a) and Fig. 7(b) display respectively the evolution of respectively the angle of attack, the flight path angle, the elevator deflection and the throttle setting during the whole manoeuver. Since the angle of attack remains in a safe domain and the considered longitudinal inputs remain by far unsaturated, this demonstrates the feasibility of the manoeuver.

In the no wind situation, the performances obtained with respect to the desired time table and the airspeed management for a delayed or an early aircraft are displayed.

Figure. 8 and Fig. 9 show airspeed and time tracking performances in two cases. The first one considers a delay situation for an aircraft according to a reference time-table where the aircraft

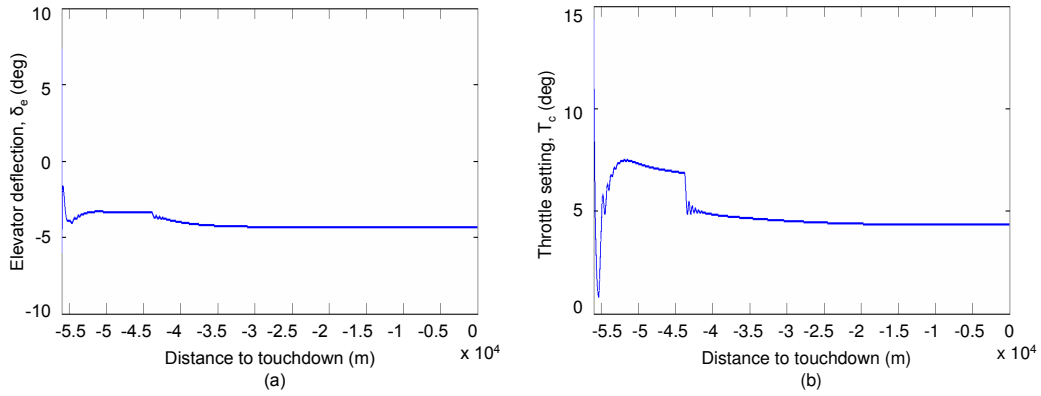

(a) Space-indexed NDI

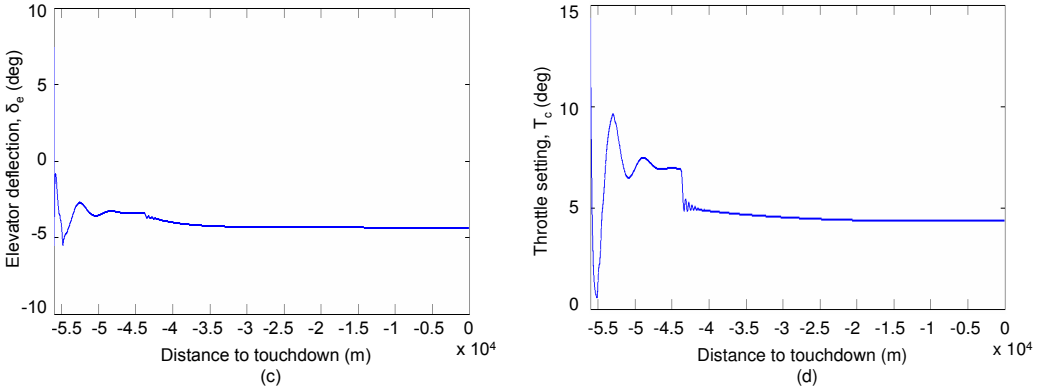

(b) Time-indexed NDI

Fig. 7 Elevator deflection and throttle setting evolution by space-indexed (a) and time-indexed (b) NDI in no wind condition.

maintains its airspeed at the maximum operating speed until it compensates the initial delay. In the second situation the aircraft is initially in advance with respect to the planned time table and in this case the speed controller sets its airspeed to the minimum allowable speed until the time tracking error is eliminated.

B. Simulation Results in the Presence of Wind

Since in this study the problem of the online estimation of the wind components has not been tackled, it has been supposed merely that the wind estimator will be similar to a first order filter with a time constant equal to 0,35s in one case (time NDI guidance) and with a space constant equal to 28m in the other case (space NDI guidance). Then the filtered values of these wind components have been fed to the respective NDI guidance control laws. Here a tailwind with a mean value of

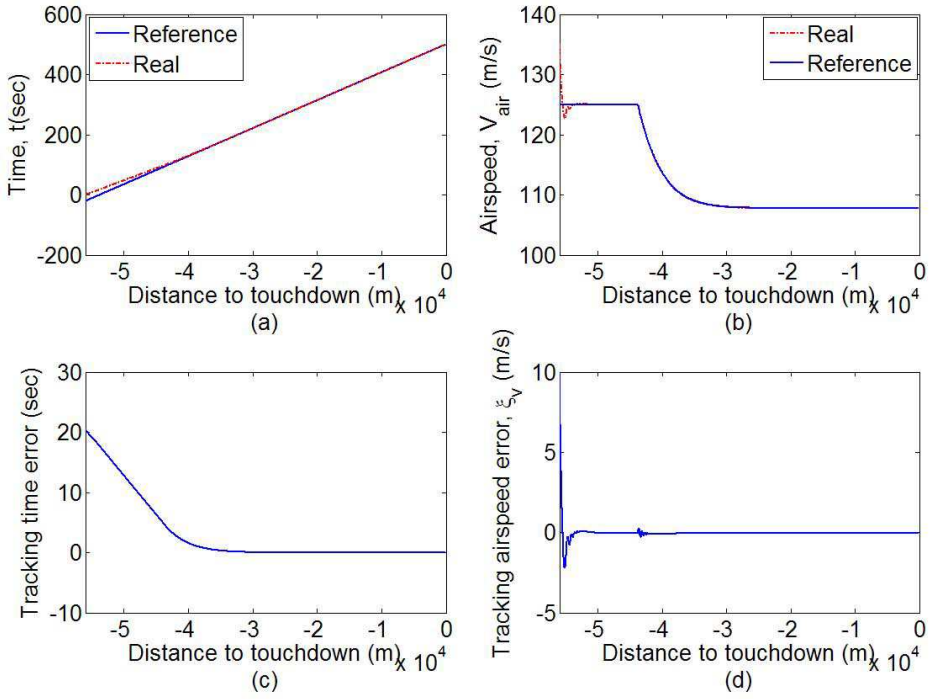

Fig. 8 Delayed initial situation and recover.

12m/s has been considered. Figure. 10 provides an example of realization of such wind.

Figure. 11 and Fig. 12 display altitude, airspeed and time tracking performances in the presence of the wind when the actual time table is late and in advance situations according to the reference time table, respectively. It appears that the proposed control technique (space-indexed NDI) keeps its performances shown in the sub-section above.

VII. Conclusion

In this paper a new longitudinal guidance scheme for transportation aircraft has been proposed. The main objective here has been to improve the tracking accuracy performance of the guidance along a desired longitudinal trajectory referenced in a spatial frame. This objective covers both vertical guidance and compliance with an overfly time table. This has led to the development of a new representation of longitudinal flight dynamics where the independent variable is ground distance to a reference point.

The nonlinear dynamic inversion control technique has been adopted in this context so that

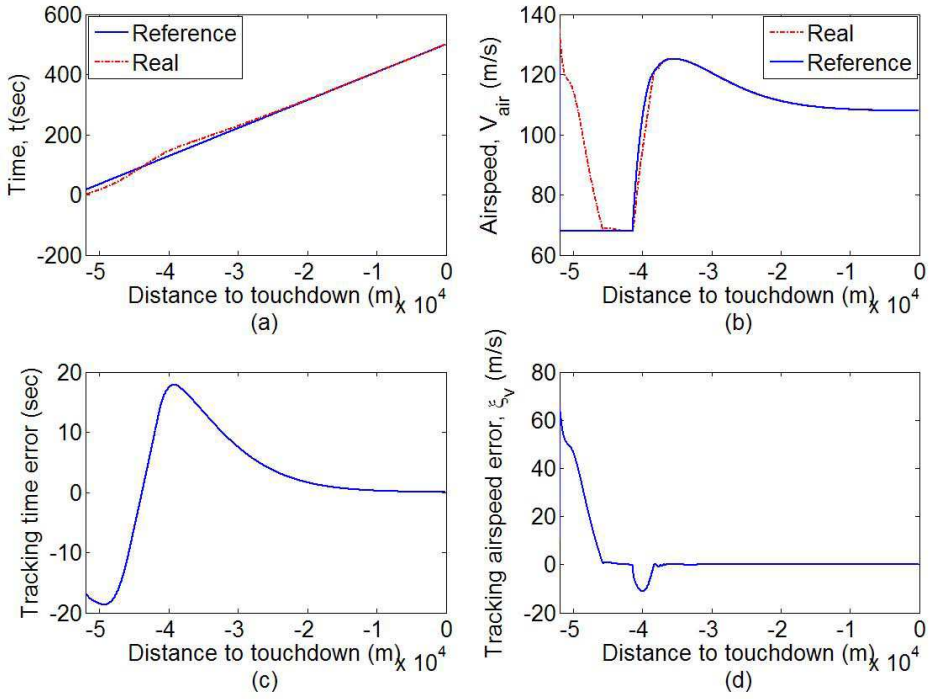

Fig. 9 Advanced initial situation and recover.

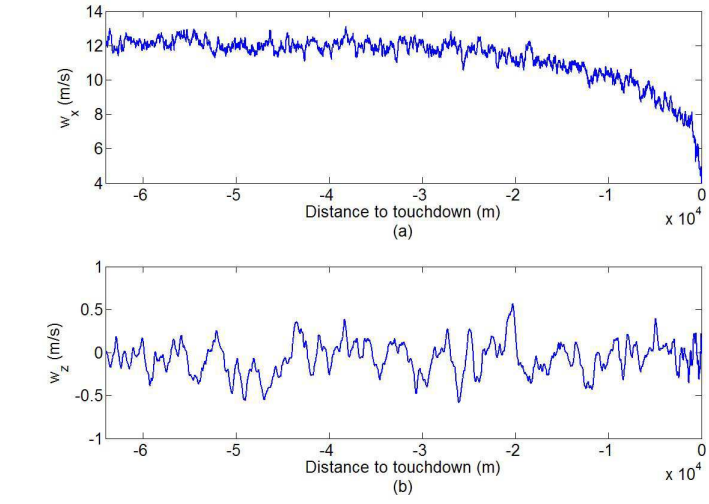

Fig. 10 Example of wind components realization.

tracking errors are made to follow independent and asymptotically stable spatial dynamics around the desired trajectories. It has been shown that a similar tracking objective expressed in the time frame cannot be equivalent when the desired airspeed changes as it is generally the case along climb and approach trajectories for landing.

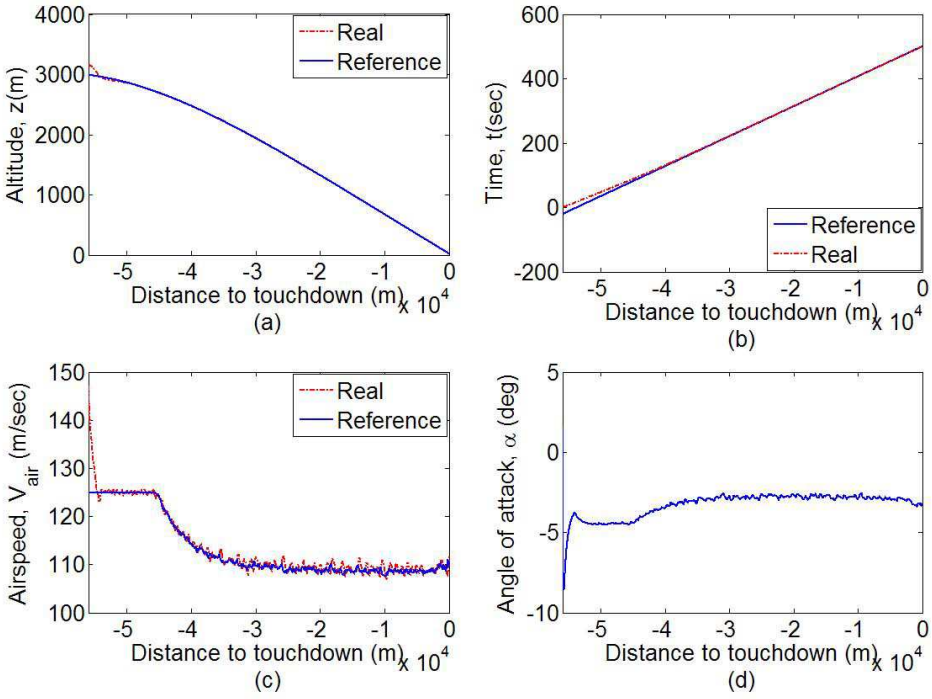

Fig. 11 Delayed initial situation and recover with wind.

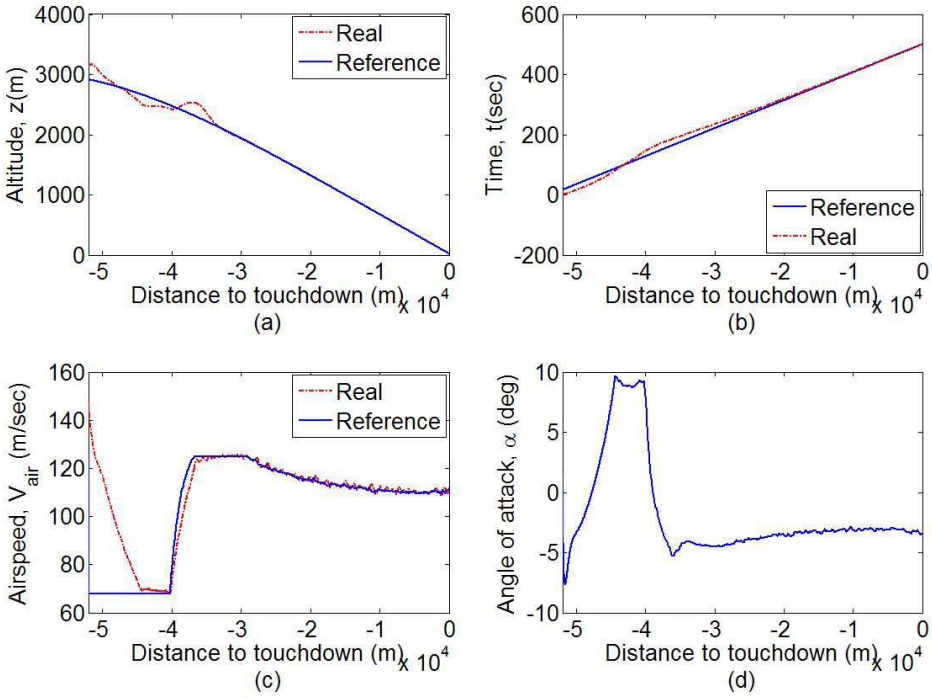

Fig. 12 Advanced initial situation and recover with wind.

The tracking performances obtained from the spatial-indexed guidance and the time-indexed NDI guidance have been compared through a simulation study considering a descent manoeuver for a transportation aircraft in wind and no wind conditions.

It appears already that the proposed approach should result in improved tracking performances as well as in better trajectory predictability, taking advantage of the enhanced capabilities of modern navigation systems while progress in online wind estimation and prediction are expected.

Appendix

The exact expressions of components A_V, B_{V_q}, B_{V_T} and A_z, B_{z_q}, B_{z_T} in Eq. (18a) and Eq. (18b) are given by:

$$\begin{aligned} A_V = \frac{1}{m}\Bigg[& -mg\dot{\gamma}_a \cos\gamma_a - \frac{T}{\tau}\cos\alpha + T\dot{\gamma}_a \sin\alpha - \rho(z)V_a\dot{V}_a SC_D + \frac{1}{2}\rho(z)V_a^3 S(C_1\dot{\gamma}_a + 2C_2\dot{\gamma}_a\alpha) \\ & + W_{xx}(\ddot{x}\cos\gamma_a - \dot{x}\dot{\gamma}_a\sin\gamma_a) + W_{xz}(\ddot{z}\cos\gamma_a - \dot{z}\dot{\gamma}_a\sin\gamma_a) - W_{zx}(\ddot{x}\sin\gamma_a + \dot{x}\dot{\gamma}_a\cos\gamma_a) \\ & - W_{zz}(\ddot{z}\sin\gamma_a + \dot{z}\dot{\gamma}_a\cos\gamma_a) + \dot{W}_{xt}\cos\gamma_a - W_{xt}\dot{\gamma}_a\sin\gamma_a - \dot{W}_{zt}\sin\gamma_a - W_{zt}\dot{\gamma}_a\cos\gamma_a \\ & - \frac{\dot{V}_a}{V_G}(-\dot{V}_a\cos\gamma_a + V_a\dot{\gamma}_a\sin\gamma_a + W_{xx}\dot{x} + W_{xz}\dot{z} + W_{xt})\Bigg] \end{aligned} \tag{34a}$$

$$B_{V_q} = \frac{1}{m}\left[-T\sin\alpha - \frac{1}{2}\rho(z)V_a^2 SC_1 - \rho(z)V_a^2 SC_2\alpha\right] \tag{34b}$$

$$B_{V_T} = \frac{1}{m\tau}\cos\alpha \tag{34c}$$

and

$$\begin{aligned} A_z = \frac{1}{V_G^2}\Bigg[& A_V(w_x\sin\gamma_a + w_z\cos\gamma_a) + F(z,\alpha,V_a,T,W)\Big\{-V_a^2 + V_a(w_x\cos\gamma_a - w_z\sin\gamma_a)\Big\} \\ & + \Upsilon(z,\alpha,V_a,T,W)V_G^2\Bigg] \end{aligned} \tag{35}$$

with $\Upsilon(z,\alpha,V_a,T,W)$ and $F(z,\alpha,V_a,T,W)$ are such as:

$$\begin{aligned}\Upsilon = \frac{1}{V_G^2}\Bigg[&-2V_a\dot{V}_a\dot{\gamma}_a + 2\dot{V}_a\dot{\gamma}_a(w_x\cos\gamma_a - w_z\sin\gamma_a) - V_a\dot{\gamma}_a^2(w_x\sin\gamma_a + w_z\cos\gamma_a)\\ &- V_a(\ddot{w}_z\cos\gamma_a + \ddot{w}_x\sin\gamma_a) + w_x(W_{zx}\ddot{x} + W_{zz}\ddot{z} + \dot{W}_{zt}) - w_z(W_{xx}\ddot{x} + W_{xz}\ddot{z} + \dot{W}_{xt})\\ &- \frac{2}{V_G}(-\dot{V}_a\cos\gamma_a + V_a\dot{\gamma}_a\sin\gamma_a + \dot{w}_x)\Bigg\{-V_a^2\dot{\gamma}_a - V_a(\dot{w}_z\cos\gamma_a + \dot{w}_x\sin\gamma_a)\\ &+ V_a\dot{\gamma}_a(w_x\cos\gamma_a + w_z\sin\gamma_a) + \dot{V}_a(w_x\sin\gamma_a - w_z\cos\gamma_a) + w_x(W_{zx}\dot{x} + W_{zz}\dot{z} + W_{zt})\\ &+ w_z(W_{xx}\dot{x} + W_{xz}\dot{z} + W_{xt})\Bigg\}\Bigg]\end{aligned} \tag{36}$$

$$\begin{aligned}F = \frac{1}{mV_a}\Bigg[&-\frac{T}{\tau}\sin\alpha - T\dot{\gamma}_a\cos\alpha + \rho(z)V_a\dot{V}_aSC_L - \frac{1}{2}\rho(z)V_a^2SC_{L_\alpha}\dot{\gamma}_a + mg\dot{\gamma}_a\sin\gamma_a\\ &- m(\ddot{w}_x\sin\gamma_a + \dot{w}_x\dot{\gamma}_a\cos\gamma_a + \ddot{w}_z\cos\gamma_a - \dot{w}_x\dot{\gamma}_a\sin\gamma_a)\\ &- \frac{m\dot{\gamma}_a}{V_G}\Bigg\{-V_a^2\dot{\gamma}_a\sin\gamma_a + \dot{V}_aw_x - V_a(W_{xx}\dot{x} + W_{xz}\dot{z} + W_{xt})\Bigg\}\Bigg]\end{aligned} \tag{37}$$

and

$$\begin{aligned}B_{z_q} = \frac{1}{V_G^2}\Bigg[&\frac{1}{m}(w_x\sin\gamma_a + w_z\cos\gamma_a)\Bigg(-T\sin\alpha - \frac{1}{2}\rho(z)V_a^2SC_1 - \rho(z)V_a^2SC_2\alpha\Bigg)\\ &+ \frac{1}{mV_a}\Bigg\{-V_a^2 + V_a(w_x\cos\gamma_a - w_z\sin\gamma_a)\Bigg\}\Bigg(T\cos\alpha + \frac{1}{2}\rho(z)V_a^2SC_{L_\alpha}\Bigg)\Bigg]\end{aligned} \tag{38a}$$

$$B_{z_T} = \frac{1}{V_G^2}\Bigg[\frac{\cos\alpha}{m\tau}(w_x\sin\gamma_a + w_z\cos\gamma_a) + \frac{\sin\alpha}{mV_a\tau}\Bigg\{-V_a^2 + V_a(w_x\cos\gamma_a - w_z\sin\gamma_a)\Bigg\}\Bigg] \tag{38b}$$

In the above equations the temporal derivatives $\dot{u}$ and $\ddot{u}$ with $u \in \{x, z, \gamma_a, V_a, w_x, w_z\}$ are related with the spatial derivatives of u by:

$$\dot{u} = u^{[1]}V_G \tag{39a}$$

$$\ddot{u} = u^{[2]}{V_G}^2 + u^{[1]}V_G^{[1]}V_G \tag{39b}$$

Appendix

In this study, longitudinal wind is expressed here according to [18, 19] as:

$$w_z = W_z(x,z,t) = \delta_z(V_a,z,t) \tag{40a}$$

$$w_x = W_x(x,z,t) = W_x(z) + \delta_x(V_a,z,t) \tag{40b}$$

where $W_x(z)$ and $\delta_{x,z}(V_a,z,t)$ represent the deterministic and stochastic components of the considered wind, respectively.

The deterministic horizontal wind speed component is expressed as:

$$W_x(z) = W_0(z) \ln\left(\frac{z}{z_0}\right) \tag{41a}$$

$$W_0(z) = W_0^* \cos(\omega z + \varphi_0) \tag{41b}$$

where ω and W_0^* denote the circular space frequency and magnitude of the considered wind component.

The stochastic wind components adopt Dryden spectrum model [19] generated from two normalized white gaussian noise processes through linear filters such as:

$$H_{\delta_x}(s) = \sigma_x \sqrt{\frac{2L_{xx}}{V_a}} \frac{1}{1 + \frac{L_{xx}}{V_a} s} \tag{42}$$

and

$$H_{\delta_z}(s) = \sigma_z \sqrt{\frac{L_{zz}}{V_a}} \frac{1 + \sqrt{3}\frac{L_{zz}}{V_a} s}{\left(1 + \frac{L_{zz}}{V_a} s\right)^2} \tag{43}$$

Here L_{xx} and L_{zz} are shape parameters (turbulence lenghts) such as:

- For $z \leq 305$m:

$$L_{xx} = \frac{z}{(0.177 + 0.0027z)^{1.2}} \tag{44a}$$

$$L_{zz} = z \tag{44b}$$

- For $z > 305$m:

$$L_{xx} = L_{zz} = 305m \tag{45}$$

where σ_x and σ_z represent standard deviations of independent processes such as:

$$\sigma_z = 0.1 W_{20} \tag{46}$$

and W_{20} is the horizontal wind speed at 20ft above ground level.

- For $z \leq 305$m:

$$\sigma_x = \frac{\sigma_z}{(0.177 + 0.0027z)^{0.4}} \tag{47}$$

- For $z > 305$m:

$$\sigma_x = \sigma_z \tag{48}$$

Time and spatial derivatives of the wind components are then given by:

$$\dot{w}_x = W_{xx}\dot{x} + W_{xz}\dot{z} + W_{xt} \tag{49}$$

with:

$$W_{xx} = \frac{\partial W_x}{\partial x} \qquad W_{xz} = \frac{\partial W_x}{\partial z} \qquad W_{xt} = \frac{\partial W_x}{\partial t} \tag{50}$$

and

$$\dot{w}_z = W_{zx}\dot{x} + W_{zz}\dot{z} + W_{zt} \tag{51}$$

with:

$$W_{zx} = \frac{\partial W_z}{\partial x} \qquad W_{zz} = \frac{\partial W_z}{\partial z} \qquad W_{zt} = \frac{\partial W_z}{\partial t} \tag{52}$$

References

[1] Pappas. G, C. Tomlin, J. Lygeros, D. Godbole and S. Sastry, "A Next Generation Architecture for Air Traffic Management Systemse," *IEEE Proceeding of the 36th Conference on Decision and Control*, December, 1997, San Diego, California, USA, pp. 2405-2411.

[2] Bernd Korn, Alexander Kuenz, *4D FMS for Increasing Efficiency of TMA Operations*, IEEE/AIAA 25th Digital Avionics Systems Conference, New York, 2006, pp. 1E4-1-1E4-8.

[3] Miele A, T. Wang, W. W. Melvin, *Guidance Strategies for Near-Optimum Takeoff Performance in Wind Shear*, Journal of Optimization Theory and Applications, 1986, Vol. 50, No. 1.

[4] Miele A, T. Wang, W. W. Melvin, "Optimization and Gamma/Theta Guidance of Flight Trajectories in a Windshear," *Presented at the 15th ICAS Congress*, 1986, London.

[5] Miele A, "Optimal Trajectories and Guidance Trajectories for Aircraft Flight Through Windshears," Honolulu, Hawaii, Proceedings of the 29th Conference on Decision and Control, 1990, pp. 737-746.

[6] Psiaki M.L. and R.F. Stengel, "Analysis of Aircraft Control Strategies for Microburst Encounter,"Journal of Guidance, Control, and Dynamics, Vol. 8, No. 5, pp. 553-559. 1985.

[7] Psiaki M.L. and K. Park, "Thrust Laws for Microburst Wind Shear Penetration,"Journal of Guidance, Control, and Dynamics, Vol. 15, No. 4, 1992.

[8] Singh S.N. and W.J. Rugh, "Decoupling in a Class of Nonlinear Systems by State Feedback," *ASME Journal of Dynamic Systems, Measurement, and Control* Series G, Vol. 94, pp. 323-329, 1972.

[9] Stengel, R.F, "Toward Intelligent Flight Control," *IEEE Trans. On Systems, Man, and Cybernetics* Vol. 23, No. 6, pp. 1699-1717. 1993.

[10] Sandeep S. Mulgund and Robert F. Stengel, "Optimal Nonlinear Estimation for Aircraft Flight Control in Wind Shear," *Automatica, Vol.32, No. 1.*, January 1996.

[11] Psiaki M.L, Control of Flight Through Microburst Wind Shear Using Deterministic Trajectory Optimization, Ph.D. Thesis, Department of Mechanical and Aerospace Engineering, Princeton University, Report No. 1787-T. 1987.

[12] Bouadi. H and F. Mora-Camino, "Space-Based Nonlinear Dynamic Inversion Control for Aircraft Continuous Descent Approach", *IEEE Evolving and Adaptive Intelligent Systems Conference*, Madrid, Spain, pp. 164-169.

[13] Bouadi. H and F. Mora-Camino, "Aircraft Trajectory Tracking by Nonlinear Spatial Inversion," *AIAA Guidance, Navigation and Control Conference*, Minneapolis, Minnesota, USA, DOI: 10.2514/6.2012-4613, pp. 1-17, August 13-16, 2012.

[14] Bouadi. H and D. Choukroun and F. Mora-Camino, "Aircraft Time-2D Longitudinal Guidance Based on Spatial Inversion of Flight Dynamics," IEEE/AIAA 31st Digital Avionics Systems Conference, Williamsburg, VA, USA, pp. 3C4-1-3C4-14, October 14-18, 2012.

[15] Magni J-F. et al, Robust Flight Control, A Design Challenge, Springer-Verlag, London.

[16] Isidori A, Nonlinear Control Systems, Springer-Verlag, Berlin.

[17] Etkin, B., *Dynamics of Atmospheric Flight*, John Wiley and Sons, Inc. . . , 1985, New York.

[18] Frost W, Bowles. R, " Wind Shear Terms in the Equations of Aircraft Motion," 1984, Journal of Aircraft, Vol. 21, No.11, pp. 866-872.

[19] Campbell C. W, May 1984, A Spatial Model of Wind Shear and Turbulence for Flight Simulation, Tech. Rep. TP-2313, NASA George C. Marshall Space Flight Centre, Alabama 35812.